Performance Analysis of Multi-User Massive MIMO Systems Subject to Composite Shadowing-Fading Environment

By

Muhammad Saad Zia

NUST201260920MSEECS61212F

Supervisor

Dr. Syed Ali Hassan

Department of Electrical Engineering

A thesis submitted in partial fulfillment of the requirements for the degree of Masters of Science in Electrical Engineering (MS EE)

In

School of Electrical Engineering and Computer Science,

National University of Sciences and Technology (NUST),

Islamabad, Pakistan.

(February 2015)

Approval

It is certified that the contents and form of the thesis entitled "**Performance Analysis of Multi-User Massive MIMO Systems Subject to Composite Shadowing-Fading Environment**" submitted by **Muhammad Saad Zia** have been found satisfactory for the requirement of the degree.

Advisor: **Dr. Syed Ali Hassan**

Signature: _____

Date: _____

Committee Member 1: **Dr. Khawar Khurshid**

Signature: _____

Date: _____

Committee Member 2: **Dr. Adnan Khalid Kiani**

Signature: _____

Date: _____

Committee Member 3: **Dr. Hassaan Khaliq Qureshi**

Signature: _____

Date: _____

Dedication

I dedicate this thesis to my parents, teachers and colleagues who helped me throughout my research phase.

Certificate of Originality

I hereby declare that this submission is my own work and to the best of my knowledge it contains no materials previously published or written by another person, nor material which to a substantial extent has been accepted for the award of any degree or diploma at NUST SEECS or at any other educational institute, except where due acknowledgement has been made in the thesis. Any contribution made to the research by others, with whom I have worked at NUST SEECS or elsewhere, is explicitly acknowledged in the thesis.

I also declare that the intellectual content of this thesis is the product of my own work, except for the assistance from others in the project's design and conception or in style, presentation and linguistics which has been acknowledged.

Author Name: **Muhammad Saad Zia**

Signature: _____

Acknowledgement

I am thankful to Allah Almighty for His blessings, which allowed me to accomplish this mile stone.

I would especially like to thank my supervisor, Dr. Syed Ali Hassan, whose guidance had been a constant companion throughout the course of this dissertation.

I would also like to thank my parents for their encouragement and moral support, which helped me get through the trying spots during this journey.

Muhammad Saad Zia

Abstract

Multiple single antenna terminals transmit simultaneously to an array of hundreds of antennas in the uplink of a multi-user massive multiple-input-multiple-output (MIMO) system. Under Rayleigh fading and lognormal shadowing, the expression for the probability density function (PDF) for signal-to-interference-plus-noise-ratio (SINR) does not exist in a closed-form, which is required to calculate the outage probability of a user. In this thesis, we first approximate the signal-to-noise ratio (SNR) for a maximum-ratio-combining (MRC) receiver by a lognormal random variable in the presence of above channel impairments. We use two different techniques; the moment matching technique and the moment generating function (MGF)-based technique for lognormal approximation of the SNR and show that the two approximation techniques perform differently under different channel conditions. Based on the lognormal approximation of the SNR, we approximate the SINRs for MRC, zero forcing (ZF), and minimum mean squared error (MMSE) receivers by lognormal random variables and provide closed-form expressions for the outage probability and capacity of the system. The approximations are validated by comparing with Monte-Carlo simulations. The effects of shadowing on the performance of the system are quantified and it is illustrated that shadowing does not average out by increasing the number

of antennas.

Table of Contents

List of Figures

List of Abbreviations

Abbreviation	Description
MIMO	Multiple input multiple output
SNR	Signal to noise ratio
SINR	Signal to interference plus noise ratio
MRC	Maximum ratio combining
ZF	Zero forcing
MMSE	Minimum mean squared error
PDF	Probability density function
CDF	Cumulative distribution function
CCDF	Complementary cumulative distribution function
MGF	Moment generating function

Chapter 1

Introduction

1.1 Introduction to MIMO Systems

Multiple-input multiple-output (MIMO) systems use multiple antennas at the transmitter and/or receiver to simultaneously transmit different data streams. Multiple antennas provide more degrees of freedom to the propagation channel and improve the throughput and link reliability. Such systems exploit the phenomenon of multipath propagation, which is traditionally a drawback in wireless communications, to the benefit of the user [1]. The improvements in the performance offered by MIMO systems are due to diversity gain, spatial multiplexing gain, array gain and interference reduction[2].

Diversity mitigates fading in a wireless link. Diversity is achieved by transmitting the same signal over independent fading paths. The receiver then combines the arriving signals in such a manner that the resultant signal formed exhibits less amplitude fluctuations. The spatial multiplexing gain results in an increase in capacity and is realized by transmitting independent data streams from individual antenna elements. The array gain depends

on the number of antennas available at the transmitter and the receiver and it results in an increase in the average received signal-to-noise ratio (SNR). Interference reduction makes possible more aggressive frequency reuse in wireless systems. The most common type of interference in a wireless system is cochannel interference which is caused by frequency reuse. By using multiple antennas, the difference between the spatial signatures of the desired signal and the cochannel signals can be used to reduce interference [2].

In general, it is not possible to make use of all the advantages of MIMO technology simultaneously due to the conflicting nature of demands placed on the spatial degrees of freedom. For instance, the spatial degrees of freedom (number of antennas) can either be used to provide diversity gain or the spatial multiplexing gain, but not both, at any one instant of time.

MIMO is a key feature of all the latest broadband systems but the deployment of MIMO on a scale that truly utilizes its potential is yet to be seen because of several reasons. The conventional point-to-point MIMO requires a rich scattering environment and expensive multiple-antenna terminals. Moreover, the complexity associated with optimal signal detection at the receiver grows exponentially with the number of antennas at the transmitter [3]-[4]. The shortcomings of a point-to-point MIMO system can be overcome by using multi-user MIMO systems which use single-antenna terminals that are served simultaneously by an antenna array [5]. Multiuser MIMO systems often employ advanced coding schemes to transmit data simultaneously to many users. However, complex interference mitigation techniques need to be used in the multi-user systems to maintain a controlled level of interuser

interference [6].

1.2 From MIMO to Massive MIMO

Massive MIMO is a novel concept that uses hundreds of antennas at the base station (BS) to serve tens of users simultaneously in the same time-frequency resource. Massive MIMO basically allows us to reap all the benefits of conventional MIMO on a huge scale. In massive MIMO systems, a large number of BS antennas improve spectral efficiency and radiated energy efficiency as compared to the existing wireless technologies. The excessive BS antennas make use of the concept of beamforming by transmitting only in the desired directions so that the radiated energy is focused in a small region and interference is minimized [7]–[8].

Massive MIMO systems allow an increase in theoretical capacity and reduction in uplink (UL) and downlink (DL) power consumption. The uplink power can be scaled down by moderately increasing the number of BS antennas [9]. In [10], a peak-to-average-power reduction (PAPR) scheme has been proposed for the downlink of large scale multiuser MIMO systems that enables the use of low cost hardware at the BS. All these reasons make massive MIMO a viable solution for future broadband technologies.

As the number of antennas at the BS increases, linear receivers such as maximum ratio combining (MRC) and minimum mean squared error (MMSE) become optimal. As a result, the acquisition of channel state information (CSI) becomes crucial for the operation of massive MIMO systems [11]–[13]. Acquisition of CSI is done through pilot sequences. Since the pilots require orthogonality between the antennas and all users operate in the

same time-frequency resource, such systems have an inherent limitation due to pilot contamination [12]. In [13], it is shown that the main limiting factor in increasing the number of BS antennas is pilot contamination.

1.3 Motivation for Massive MIMO

With a large number of BS antennas, things that were random before, now start to look deterministic. As a consequence, thermal noise and small-scale fading are averaged out in massive MIMO systems. Theoretically, if the number of antennas is allowed to grow without bound, the uncorrelated noise and intracell interference disappear completely [5]. However, the effects of shadowing still remain. Shadowing in wireless systems is known to follow a lognormal distribution. Under Rayleigh fading and lognormal shadowing, the expressions for the probability density function (PDF) of signal-to-interference-plus-noise-ratio (SINR) for massive MIMO systems do not exist in a closed-form. Closed-form expressions for SINR are needed to calculate the outage probability and capacity of the system. However, it is known that a sum or product distribution involving lognormal random variables (RVs) can be well-approximated by a new lognormal RV [14]. The new lognormal RV can then be used to calculate the outage probability and capacity of a system.

1.4 Problem Statement

To analyze and quantify the effects of large-scale fading on the uplink performance of multiuser massive MIMO systems and provide closed-form expres-

sions for the PDF of SINR to calculate the outage and capacity for MRC, zero forcing (ZF) and MMSE receivers under composite shadowing-fading environment.

1.5 Thesis Contribution

In this research work, we develop a system model for a multiuser massive MIMO system operating under a composite fading environment. We analyze the SINR for three linear receivers, namely MRC, ZF and MMSE. We provide closed-form expressions for the PDF of SINR for the three receivers under composite fading environment. The closed-form expressions for the PDF of SINR are obtained by approximating the SINR by a lognormal RV. We also establish the lower bounds on the uplink achievable rates. At the end, we quantify the effects of shadowing on the uplink performance of multiuser massive MIMO systems.

1.6 Thesis Organization

The rest of the thesis is organized as follows: Chapter 2 presents the related work on composite fading environments in massive MIMO systems. In chapter 3, we present the system model for a massive MIMO system subject to a composite shadowing-fading environment. The fading distributions are also given in chapter 3. Chapter 4 presents the SNR and SINR analysis of an MRC receiver. The analyses for ZF and MMSE receivers are given in chapter 5. Simulation results and discussions on performance analysis follow in chapter 6. Finally, conclusions and future work are presented in chapter 7.

Chapter 2

Literature Review

Most of the previous work on MIMO channels considers small-scale fading only. For instance, in [15]-[19], the authors' have chosen Rayleigh-fading channels to investigate the asymptotic performance of MIMO systems. Similarly, in [20]-[24], the focus of the authors was on Rician fading channels to derive ergodic capacity of MIMO systems. Regarding composite fading environments, some work appears in [25] where a composite nakagami-lognormal channel is chosen to obtain lower bounds on the capacity of a distributed MIMO system. All of these works focus on the capacity of the system and do not analyze or address the outage probability under the stated channel conditions.

To the best of our knowledge, no work has been done that analyzes the effects of large-scale fading on massive MIMO systems. In [26], the authors focus on the impacts of large-scale fading on the uplink of massive MIMO systems from the perspective of ergodic capacity considering generalized-$\mathcal{K}$ fading channels. $\mathcal{K}$-fading channels are composite fading channels in which the small-scale fading is modeled via Nakagami-m distribution and the large-scale

fading via the gamma distribution [26]-[27]. The approximation of lognormal shadowing by a gamma distribution helps in the performance evaluation of composite fading channels by providing closed-form expressions for the PDF of the composite channel which otherwise does not exist in a closed-form.

In [9], exact lower bounds have been derived for the capacity of linear receivers in massive MIMO systems operating under composite fading environment, but these bounds do not incorporate the PDF of lognormal distribution, instead, the lognormal shadowing is averaged out by performing Monte-Carlo simulations, which limits the analysis of such systems operating under shadowing environments. In [28], the authors proposed a channel estimation scheme for massive MIMO with *a priori* knowledge of shadowing. This is because the closed-form expression for the PDF of SINR under composite fading and shadowing environment is prohibited for very large number of antennas. The case of SNR under Rayleigh fading and lognormal shadowing has been investigated in [29], however, the expression for received power involves a sum of a small number of Suzuki RVs, which does not apply serve our purpose of obtaining closed-form expression of SINR for to the massive MIMO systems.

The authors in [33] incorporate large-scale fading in their system model to derive lower bounds on the SINR for an minimum-mean-squared-error (MMSE) receiver asymptotically, but do not give an exact PDF of SINR for outage calculation. Similarly, in [34], the effects of large-scale fading on a zero forcing (ZF) receiver have been analyzed for a finite number of BS antennas but the analysis of MMSE is left out due to its challenging mathematical nature.

Chapter 3

System Model for Multi-User Massive MIMO Systems

In this chapter, we develop the system model for a very large scale multi-user MIMO system operating under a composite fading environment. The small-scale fading arises due to the presence of multiple propagation paths between the transmitter and the receiver. The difference in the propagation delay of each path causes a change in the phase of the waves arriving at the receiver antennas. This change of phase causes the received signals from the multiple paths to undergo constructive or destructive interference at the receiver. The large-scale fading is caused by the presence of an obstacle in the propagation path and depends on the environmental surroundings and the transmitter-receiver separation distance. The two types of fading are responsible for fluctuations in the received power. The small-scale fading causes rapid fluctuations in the received power over a short interval of time or a short travel distance whereas the large-scale fading defines the local mean of the received power at a specific transmitter-receiver distance [37]. As the

distance changes significantly or the propagation path is obstructed by an obstacle, the large-scale fading causes the local mean of the received power to deviate sufficiently from its previous value, thus defining a new local mean for that specific propagation scenario. The large-scale fading varies slowly with time.

In this thesis, we choose Rayleigh fading model to represent the small-scale fading (simply known as fading) whereas the large-scale fading (also referred to as shadowing) is modeled via lognormal distribution[30], [31]. In section 3.1, we develop a mathematical model of the wireless channel under composite Rayleigh fading-lognormal shadowing environment and in section 3.2, we formulate the received SINR for a multi-user massive MIMO system.

3.1 Channel Model

We consider the uplink of a single cell multi-user massive MIMO system where a BS is equipped with M antennas. The BS receives the data from K single-antenna users in the same time-frequency resource. These transmissions are corrupted by the channel impairments. The transmissions from K users to the BS suffer from independent Rayleigh fading and lognormal shadowing. The $M \times 1$ received signal vector at the BS is given by

$$\boldsymbol{y} = \sqrt{P_t}\boldsymbol{G}\boldsymbol{x} + \boldsymbol{n}, \tag{3.1}$$

where $\boldsymbol{G}$ represents the $M \times K$ channel matrix between the K users and the M BS antennas, P_t is the average transmit power of a single user, $\boldsymbol{x}$ is the vector of symbols transmitted simultaneously by K users and $\boldsymbol{n}$ is the noise vector.

The channel matrix $\boldsymbol{G}$ models Rayleigh fading and lognormal shadowing. The channel coefficient g_{ik} between the ith BS antenna and the kth user can be represented as

$$g_{ik} = h_{ik}\sqrt{\nu_k}, \tag{3.2}$$

where h_{ik} is the small-scale fading coefficient between the ith BS antenna and the kth user and ν_k represents the large-scale fading of the kth user such that $\nu_k \sim Log\ \mathcal{N}(\mu_{(dB)}, \sigma^2_{(dB)})$. In a Rayleigh fading environment, the small-scale fading coefficient h_{ik} follows a complex normal distribution with zero mean and unit variance i.e., $h_{ik} \sim \mathcal{CN}(0, 1)$.

Since the BS antennas are closely spaced, the large-scale fading for a single user across M BS antennas is correlated. However, the small-scale fading coefficients are independent and identically distributed (i.i.d). In this thesis, we assume perfect correlation between the shadowing components of a single user across M BS antennas. Therefore, the received signals from the kth user across M BS antennas suffer identical shadowing. The channel matrix $\boldsymbol{G}$ is then given by

$$\boldsymbol{G} = \boldsymbol{H}\boldsymbol{V}^{1/2}, \tag{3.3}$$

where $\boldsymbol{H}$ is the $M \times K$ matrix of small-scale fading coefficients between the M BS antennas and K users and $\boldsymbol{V}$ is a $K \times K$ diagonal matrix containing the large-scale fading coefficients of K users. By using a linear detector, the received signal $\boldsymbol{y}$ is processed as

$$\boldsymbol{r} = \boldsymbol{A}^H\boldsymbol{y}. \tag{3.4}$$

The vector $\boldsymbol{r}$ in (3.4) gives the received signals from all the users where $\boldsymbol{A}$ is the linear detector matrix that depends on the channel matrix $\boldsymbol{G}$ and H is the Hermitian operator.

3.2 SINR Formulation

After applying the linear detector and from (3.4), the received signal vector is given by

$$\boldsymbol{r} = \sqrt{P_t}\boldsymbol{A}^H\boldsymbol{G}\boldsymbol{x} + \boldsymbol{A}^H\boldsymbol{n}. \tag{3.5}$$

To formulate the SINR of a single user, the vector $\boldsymbol{r}$ is decomposed into two parts. Let r_j and x_j represent the received signal and the transmitted symbol of the jth user, respectively. Then

$$r_j = \sqrt{P_t}\boldsymbol{a}_j^H\boldsymbol{g}_j x_j + \sqrt{P_t}\sum_{k=1,k\neq j}^{K}\boldsymbol{a}_j^H\boldsymbol{g}_k x_k + \boldsymbol{a}_j^H\boldsymbol{n}, \tag{3.6}$$

where $\boldsymbol{a}_j$ and $\boldsymbol{g}_j$ represent the jth columns of the matrices $\boldsymbol{A}$ and $\boldsymbol{G}$, respectively. The first term in (3.6) represents the desired signal of the jth user, whereas the other two terms constitute interference from other users and noise, respectively. Without the loss of generality, we assume unit power spectral density of noise. The SINR of the jth user can then be represented as

$$SINR_j = \frac{P_t|\boldsymbol{a}_j^H\boldsymbol{g}_j|^2}{P_t\sum_{k=1,k\neq j}^{K}|\boldsymbol{a}_j^H\boldsymbol{g}_k|^2+\|\boldsymbol{a}_j\|^2}. \tag{3.7}$$

where $\|.\|$ represents the 2-norm of a vector and $|.|$denotes the absolute value of a vector.

3.3 Fading Distributions

3.3.1 Rayleigh Fading Distribution

In a rich scattering environment, if there is no dominant line-of-sight path between the transmitter and the receiver, the magnitude, R, of the received

signal's complex envelope follows a Rayleigh distribution [38]. The PDF of the Rayleigh distribution is given by

$$P_R(r) = \frac{2r}{\Omega_p} \exp\left(-\frac{r^2}{\Omega_p}\right), \qquad r \geq 0. \tag{3.8}$$

where Ω_p is the average envelope power. In terms of channel coefficients, the magnitude of complex envelope can be written as $R = |h_{ik}|$.

In wireless communications, the corresponding squared envelope of the received signal is of considerable importance as it is directly proportional to the received power and thus, represents the received SNR [31]. The square of a Rayleigh RV is an exponential RV. The squared envelope, R^2, thus follows an exponential distribution with the PDF given by

$$P_{R^2}(r) = \frac{1}{\Omega_p} \exp\left(-\frac{r}{\Omega_p}\right), \qquad r \geq 0. \tag{3.9}$$

For simulation purposes, the average envelope power has to be kept unity [31]. Therefore, we assume $\Omega_p = 1$ throughout the thesis. The distribution of the squared envelope can then be represented as $|h_{ik}|^2 \sim Exp(1)$.

3.3.2 Lognormal Shadowing Distribution

Practical measurements have shown that the local mean of the received power follows a lognormal distribution, therefore, the received squared envelope due to shadowing in wireless communications is often modeled by a lognormal RV [31], [32]. The PDF of the lognormal distribution is given by

$$P_V(\nu) = \frac{\xi}{\nu\sigma_{(dB)}\sqrt{2\pi}} \exp\left(-\frac{\left(\xi \log_e \nu - \mu_{(dB)}\right)^2}{2\sigma_{(dB)}}\right) \tag{3.10}$$

where $\xi = 10/\log_e 10$ is a scaling constant and $\sigma_{(dB)}$ is the shadow standard deviation. The lognormal RV, V, in (3.10) is defined as $V = 10^{0.1X}$ such that

$X \sim \mathcal{N}(\mu_{(dB)}, \sigma^2_{(dB)})$. The typical value of $\sigma_{(dB)}$ lies between 4 dB and 12 dB. The higher the value of $\sigma_{(dB)}$, the more severe the shadowing is.

Chapter 4

Analysis of MRC Receiver

In this chapter, we analyze the MRC receiver for a very large scale multi-user MIMO system under a composite-fading environment. We use (3.7) in the context of an MRC receiver to analyze the SINR.

In case of perfect CSI, the $M \times K$ linear detector matrix $\boldsymbol{A}$ for an MRC receiver is given by $\boldsymbol{A} = \boldsymbol{G}$ hence $\boldsymbol{a}_j = \boldsymbol{g}_j$. From (3.3) and (3.7), we obtain the SINR of a single user for an MRC receiver as

$$\begin{aligned} SINR_j^{mrc} &= \frac{P_t \|\boldsymbol{h}_j\|^4 \nu_j^2}{P_t \nu_j \sum_{k=1,k\neq j}^{K} |\boldsymbol{h}_j^H \boldsymbol{h}_k|^2 \nu_k + \|\boldsymbol{h}_j\|^2 \nu_j} \\ &\triangleq \frac{P_t \|\boldsymbol{h}_j\|^2 \nu_j}{P_t \sum_{k=1,k\neq j}^{K} \frac{|\boldsymbol{h}_j^H \boldsymbol{h}_k|^2}{\|\boldsymbol{h}_j\|^2} \nu_k + 1}. \end{aligned} \tag{4.1}$$

Conditioned on $\boldsymbol{h}_j$, we define a new RV $\tilde{g}_k$ such that $\tilde{g}_k = \frac{|\boldsymbol{h}_j^H \boldsymbol{h}_k|}{\|\boldsymbol{h}_j\|}$. $\tilde{g}_k$ is a Gaussian RV with zero mean and unit variance that is independent of $\boldsymbol{h}_j$. Therefore, $\tilde{g}_k \sim \mathcal{CN}(0,1)$. From (4.1), the SINR is then given by

$$SINR_j^{mrc} = \frac{P_t \|\boldsymbol{h}_j\|^2 \nu_j}{P_t \sum_{k=1,k\neq j}^{K} |\tilde{g}_k|^2 \nu_k + 1}. \tag{4.2}$$

We now derive the PDF of the SNR and SINR in the following sections.

4.1 SNR of MRC Receiver

The numerator in (4.2) is the SNR, Z, of a single user at the BS. For notational simplicity, we omit the subscripts in the expression of Z. Therefore,

$$Z = P_t\ \nu \sum_{i=1}^{M} |h_i|^2 := P_t\ \nu\ \gamma, \tag{4.3}$$

where $\gamma \sim \Gamma(M, 1)$ owing to the sum of independent and identically distributed (i.i.d.) exponential RVs each having a unit mean.

From (4.3), it is evident that the SNR follows a gamma-lognormal product distribution. The PDF of a gamma RV is given by

$$P_G(\gamma) = \frac{\gamma^{M-1} \exp(-\gamma)}{\Gamma(M)}, \tag{4.4}$$

where $\Gamma(M) = (M-1)!$ since M is an integer. The distribution of a product RV, $Z = VG$, is given by

$$P_Z(z) = \int_{-\infty}^{\infty} P_V(\nu) P_G\left(\frac{z}{\nu}\right) \frac{1}{|\nu|} d\nu. \tag{4.5}$$

Since, P_t is a constant, therefore, we neglect it in the PDF expression of gamma-lognormal product distribution. From (4.5), the PDF of the product of gamma and lognormal RVs is then given by

$$P_Z(z) = \frac{\xi z^{M-1}}{(M-1)!\ \sigma_{(dB)}\sqrt{2\pi}} \int_0^{\infty} \frac{\exp(-z/\nu)}{\nu^{(M+1)}} \exp\left(\frac{-\left(\xi \log_e \nu - \mu_{(dB)}\right)^2}{2\sigma_{(dB)}^2}\right) d\nu, \tag{4.6}$$

From (4.6) it can be noticed that the PDF of SNR does not exist in a closed-form. However, the product distribution in (4.6) can be approximated by a new lognormal RV, $Y = 10^{0.1X}$ such that $X \sim \mathcal{N}(\mu_X, \sigma_X^2)$ and $Y \sim Log\ \mathcal{N}(\mu_X, \sigma_X^2)$.

In the following sections, we propose two methods to approximate the PDF of SNR (gamma-lognormal product distribution) by another lognormal RV. As the lognormal distribution is completely characterized by two parameters, namely the *mean* and *variance* of the associated Gaussian RV, hence the product distribution can be approximated by the lognormal distribution by finding the mean and variance of the Gaussian RV associated with the approximating lognormal RV.

4.1.1 Moment Matching Method for lognormal approximation of the PDF of SNR

In this method, the first and second central moments of the Gaussian RV X_1 associated with the approximating lognormal RV, $Y_1 = 10^{0.1X_1}$, are equated with the corresponding moments of the product RVs. The mean, μ_{X_1}, associated with the approximating lognormal distribution is given by

$$\begin{aligned}\mu_{X_1} &= \mathbb{E}\{10\log_{10} Z\},\\ &\triangleq \frac{\xi}{\sigma_{(dB)}\sqrt{2\pi}\,(M-1)\,!}\int_0^\infty\int_0^\infty (10\log_{10} Z)\frac{z^{M-1}}{\nu^{M+1}}\\ &\quad\times \exp\left(\frac{-z}{\nu}\right)\exp\left(-\frac{\left(\xi\ln\nu-\mu_{(dB)}\right)^2}{2\sigma_{(dB)}^2}\right)d\nu dz,\end{aligned} \tag{4.7}$$

where $\mathbb{E}$ is the expectation operator. Solving the inner integral with respect to z in (4.7) yields

$$\mu_{X_1} = \frac{\xi^2}{\sigma_{(dB)}\sqrt{2\pi}} \int_0^\infty \frac{1}{\nu} \left\{\psi(M) + \ln(\nu)\right\} \exp\left(-\frac{\left(\xi \ln \nu - \mu_{(dB)}\right)^2}{2\sigma^2_{(dB)}}\right) \, d\nu, \tag{4.8}$$

where $\psi(M) = -0.5772 + \sum_{k=1}^{M-1} \frac{1}{k}$.

After substituting $\xi \ln \nu = z$ in (4.8) and doing considerable algebraic manipulation, the final expression for the mean associated with the approximating lognormal RV, Y_1, is given as

$$\mu_{X_1} = \xi\psi(M) + \mu_{dB}. \tag{4.9}$$

The variance of X_1 is calculated from its second moment. The second moment of X_1 is given as

$$\begin{aligned} \mathbb{E}\{(10\log_{10} Z)^2\} = \frac{\xi}{\sigma_{(dB)}\sqrt{2\pi}(M-1)!} \int_0^\infty \int_0^\infty \frac{z^{M-1}}{\nu^{M+1}} \exp\left(\frac{-z}{\nu}\right) \\ \times \exp\left(-\frac{(\xi \ln \nu - \mu_{dB})^2}{2\sigma^2_{dB}}\right) \left\{(10\log_{10} Z)^2\right\} d\nu dz. \end{aligned} \tag{4.10}$$

Using the approach used in the derivation of μ_{X_1} and solving the inner integral with respect to z in (4.10) yields

$$\begin{aligned} \mathbb{E}\{(10\log_{10} Z)^2\} = \frac{\xi^3}{\sigma\sqrt{2\pi}} \int_0^\infty \exp\left(-\frac{(\xi \ln \nu - \mu_{dB})^2}{2\sigma^2_{dB}}\right) \\ \times \frac{1}{y} \left\{ \left(\psi(M) - \ln(\frac{1}{y})\right)^2 + \zeta(2, M) \right\} d\nu, \end{aligned} \tag{4.11}$$

where $\zeta(2, M) = \sum_{k=0}^{\infty} \frac{1}{(M+k)^2}$, is the Riemann-zeta function.

Substituting $\xi \ln \nu = z$ in (4.11) and doing hefty algebra gives the second moment of X_1 as

$$\begin{aligned} \mathbb{E}\{(10\log_{10} Z)^2\} = \xi^2 \left(\psi(M)\right)^2 + 2\xi\psi(M)\mu_{dB} \\ + \xi^2\zeta(2, M) + \mu^2_{dB} + \sigma^2_{dB}. \end{aligned} \tag{4.12}$$

Having obtained the first and second moments of X_1, the variance of X_1 is given as

$$\begin{aligned}\sigma_{X_1}^2 &= \mathbb{E}\{(10\log_{10} Z)^2\} - (\mathbb{E}\{10\log_{10} Z\})^2 \\ &\triangleq \sigma_{dB}^2 + \xi^2\zeta(2, M).\end{aligned} \tag{4.13}$$

The gamma-lognormal product distribution can now be approximated by $Y_1 = 10^{0.1X_1}$ where $X_1 \sim \mathcal{N}(\mu_{X_1}, \sigma_{X_1}^2)$ and μ_{X_1} and σ_{X_1} are in dB.

4.1.2 MGF-based method for lognormal approximation of the PDF of SNR

In this method, the moment generating functions (MGFs) of the approximating lognormal RV, Y_2, and the product RVs are equated to find the parameters μ_{X_2} and $\sigma_{X_2}^2$of $Y_2 = 10^{0.1X_2}$. However, the MGFs of both the lognormal and the product RVs do not exist in closed-form but they can be computed numerically by applying Gauss-Hermite integration.

The MGF of Y_2 is given as

$$\Psi_{Y_2}(s) = \int_0^\infty \exp(-sy) P_{Y_2}(y)\ dy, \tag{4.14}$$

where $P_{Y_2}(y) = \frac{\xi}{y\sigma_{X_2}\sqrt{2\pi}} \exp\left(\frac{-\left(\xi\log_e y - \mu_{X_2}\right)^2}{2\sigma_{X_2}^2}\right)$ is the logormal PDF.

Substituting $p = \frac{\xi\log_e y - \mu_{X_2}}{\sqrt{2}\sigma_{X_2}}$ in $P_{Y_2}(y)$, (4.14) can be rewritten as

$$\Psi_{Y_2}(s) = \int_{-\infty}^\infty \frac{1}{\sqrt{\pi}} \exp\left(-p^2\right) \exp\left[-s\exp\left(\frac{\sqrt{2}p\sigma_{X_2} + \mu_{X_2}}{\xi}\right)\right] dp. \tag{4.15}$$

Equation (4.15) takes the form of a Hermite polynomial, thus applying Gausss-Hermite integration to (4.15) results in

$$\Psi_{Y_2}(s; \mu_{X_2}, \sigma_{X_2}) = \sum_{t=1}^{T} \frac{w_t}{\sqrt{\pi}} \exp\left[-s\exp\left(\frac{\sqrt{2}a_t\sigma_{X_2} + \mu_{X_2}}{\xi}\right)\right], \tag{4.16}$$

where a_t are the roots (abscissas) of the Hermite Polynomial and w_t are corresponding weights and T is the Hermite integration order. A higher value of T corresponds to greater accuracy.

The MGF of the product of gamma and lognormal RVs is given by

$$\Psi_Z(s) = \int_0^\infty \exp(-sz) P_Z(z)\, dz. \tag{4.17}$$

Substituting (4.6) in (4.17), we obtain

$$\begin{aligned}\Psi_Z(s) = \frac{\xi}{\sigma_{(dB)}\sqrt{2\pi}\,(M-1)\,!} \int_0^\infty \int_0^\infty \frac{z^{M-1}}{\nu^{M+1}} \exp(-sz) \exp\left(\frac{-z}{\nu}\right) \\ \times \exp\left(\frac{-\left(\xi \log_e \nu - \mu_{(dB)}\right)^2}{2\sigma_{(dB)}^2}\right) d\nu dz.\end{aligned} \tag{4.18}$$

Following a similar course of action as used to obtain (4.7) and solving the inner integral with respect to z in (4.18) results in

$$\Psi_Z(s) = \frac{\xi}{\sigma_{(dB)}\sqrt{2\pi}} \int_0^\infty \frac{1}{\nu} \frac{1}{(1+s\nu)^M} \exp\left(\frac{-\left(\xi \log_e \nu - \mu_{(dB)}\right)^2}{2\sigma_{(dB)}^2}\right) d\nu. \tag{4.19}$$

Substituting $q = \frac{\xi \ln \nu - \mu_{(dB)}}{\sigma_{(dB)}\sqrt{2}}$ in (4.19) and simplifying the expression gives

$$\Psi_Z(s) = \frac{1}{\sqrt{\pi}} \int_{-\infty}^\infty \exp\left(-q^2\right) \frac{1}{\left[1 + s\exp\left(\frac{q\sqrt{2}\sigma_{(dB)} + \mu_{(dB)}}{\xi}\right)\right]^M} dq. \tag{4.20}$$

Applying Gauss-Hermite integration to (4.20) gives the closed-form expression for the MGF of product of gamma and lognormal RVs as

$$\Psi_Z(s; \mu_{(dB)}, \sigma_{(dB)}) = \frac{1}{\sqrt{\pi}} \sum_{t=1}^{T} \frac{w_t}{\left[1 + s\exp\left(\frac{a_t\sqrt{2}\sigma_{(dB)} + \mu_{(dB)}}{\xi}\right)\right]^M}. \tag{4.21}$$

The parameters of the approximate lognormal RV can then be calculated by equating (4.16) and (4.21) at two distinct positive and real values of s,

identified by s_1 and s_2. This forms a system of two non-linear equations given by

$$\sum_{t=1}^{T} \frac{w_t}{\sqrt{\pi}} \exp\left[-s_i \exp\left(\frac{\sqrt{2}\sigma_{X_2} a_t + \mu_{X_2}}{\xi}\right)\right] = \Psi_Z(s; \mu_{(dB)}, \sigma_{(dB)}) \qquad (4.22)$$

for i=1 and 2.

The non-linear system of equations in (4.22) can be solved for μ_{X_2} and σ_{X_2}using a numerical routine. The values of s_1 and s_2 have significant effect on the performance of this approximation method. It is found that the optimal results are achieved when s_1, $s_2 \in (0, 1]$.

4.1.3 Simulation results for lognormal approximaion of the PDF of SNR

In this section, we plot the cumulative distribution function (CDF) and the complementary CDF (CCDF) to verify the accuracy of the two proposed methods to approximate the PDF of SNR for MRC receiver.

Simulations performed to verify the accuracy of the two proposed methods consider 500 BS antennas. Optimal values of $s_1 = 0.001$ and $s_2 = 0.005$ have been chosen for these simulations. The results of the two proposed methods are compared with Monte-Carlo simulations of the product of gamma and lognormal RVs. For simulations, we multiplied the Rayleigh and lognormal RVs according to (3.7) and averaged them over 10^7 Monte-Carlo trials.

Fig. 4.1 shows the CDF and the CCDF of SNR for the MRC receiver obtained through both the moment matching approach and the MGF-based approach along with the simulations. It can be seen that the proposed methods approximate the product of gamma and lognormal RVs with a good

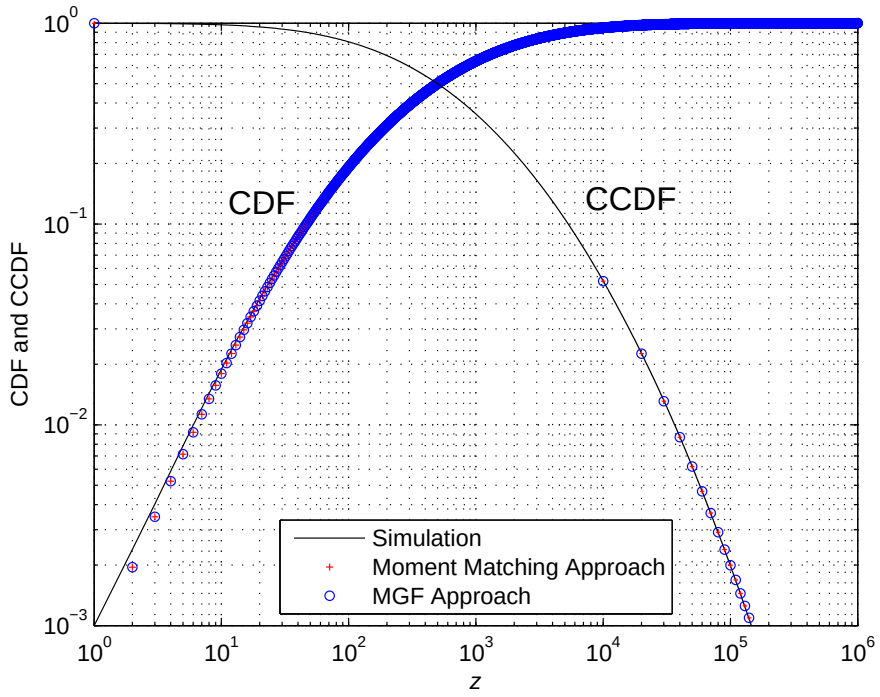

Figure 4.1: Comparison of accuracy CDF and CCDF of the two proposed methods $\left(\mu_{(dB)} = 0 \text{ and } \sigma_{(dB)} = 8\right)$

accuracy. Both methods have greater accuracy in approximating the CCDF as compared to the CDF.

Greater accuracy in approximating the CCDF implies that both the proposed methods approximate the tail of the gamma-lognormal product PDF precisely. The tail of the gamma-lognormal PDF is particularly important in calculating the outage probability of the system. The mean absolute error (MAE) of both the proposed methods is of the order of 10^{-8}. Though the value of MAE is very small for both the approximating methods, it becomes significant in applications where a high degree of precision is required. While calculating the outage probability for massive MIMO systems, we need an

approximation of the gamma-lognormal PDF with the least MAE. However, as the channel conditions ($\mu_{(dB)}$ and $\sigma_{(dB)}$) vary, the accuracy of the two approximation approaches also varies.

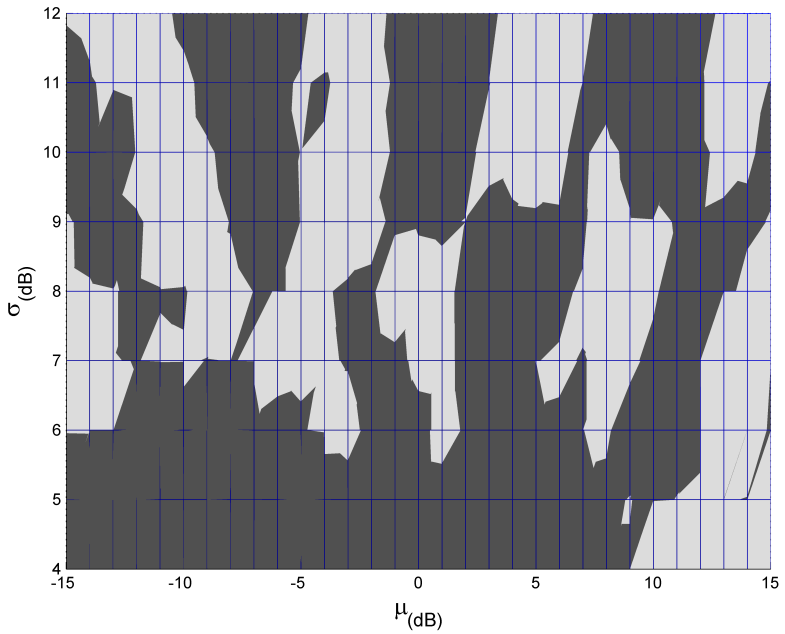

Figure 4.2: Performance regions of MM and MGF techniques

Fig. 4.2 shows various combinations of $\mu_{(dB)}$ and $\sigma_{(dB)}$ where the moment matching and MGF approaches perform better than one another. From the perspective of channel modeling, typical values of $\sigma_{(dB)}$ are from 4 to 12, whereas negatives values of $\mu_{(dB)}$ are of considerable importance when the path loss is taken into account in (3.3).

The darker portions in 4.2 show the regions where the MGF approach performs better and the lighter portions show the regions where the moment matching approach performs better. However, the difference between the performance of these two approaches is of the order of 10^{-12} in terms of

MAE.

4.2 SINR of MRC Receiver

Based on the lognormal approximation of SNR, the SINR of an MRC receiver can also be approximated by a lognormal RV. Approximating the SINR by a lognormal RV is based on the two above mentioned approximating methods. The summation in the denominator of (4.2) involves a product of exponential and lognormal RVs. Since gamma RV is a sum of i.i.d. exponential RVs, substituting $M = 1$ in (4.6) gives the PDF of the product of exponential and lognormal RVs as

$$P_Z(z) = \frac{\xi}{\sigma_{(dB)}\sqrt{2\pi}} \int_0^\infty \frac{\exp\left(-z/\nu\right)}{\nu^2} \exp\left(\frac{-\left(\xi \log_e \nu - \mu_{(dB)}\right)^2}{2\sigma_{(dB)}^2}\right) d\nu, \quad (4.23)$$

From (4.23), it is clear that the distribution of the product of these RVs also does not exist in a closed-form. However, like the gamma-lognormal product distribution, the exponential-lognormal product distribution can be approximated by another lognormal RV, $W \sim \text{Log-}\mathcal{N}(\mu_a, \sigma_a^2)$. Substituting $M = 1$ in (4.9) and (4.13) gives the parameters of W through the moment-matching technique. The sum of K independent approximating lognormal RVs, W, can then be approximated by yet another lognormal RV by the MGF method [14].

Alternatively, substituting $M = 1$ in (4.21) gives the MGF of the product of exponential and lognormal RVs. This MGF is the same as the MGF of a

Suzuki RV, S_k, given in [14]. The MGF of S_k is given by

$$\Psi_{S_k}(s;\mu_{(dB)},\sigma_{(dB)}) = \frac{1}{\sqrt{\pi}}\sum_{t=1}^{T}\frac{w_t}{1+s\exp\left(\frac{a_t\sqrt{2}\sigma_{(dB)}+\mu_{(dB)}}{\xi}\right)}. \tag{4.24}$$

In [14], the authors have proposed an MGF-based method to approximate the sum of K independent Suzuki RVs by a new lognormal RV. The proposed method equates the MGF of approximating lognormal RV with the product of MGFs of Suzuki RVs. We use the same proposed method to serve our purpose and approximate the sum of product of exponential and lognormal RVs by a new RV, $R \sim \text{Log-}\mathcal{N}(\mu_b, \sigma_b^2)$. According to the MGF-based method,

$$\Psi_R(s_i;\mu_b,\sigma_b) = \prod_{k=1}^{K}\Psi_{S_k}(s_i;\mu_{(dB)},\sigma_{(dB)}) \quad \text{at } i\text{=1 and 2.} \tag{4.25}$$

where Ψ_R is the MGF of the approximating lognormal RV and is the same as given by (4.16). In (4.25), μ_b and σ_b are the unknowns whereas the right hand side of the equation consists completely of known quantities and Ψ_{S_k} is evaluated at $s_1 = 1.0$ and $s_2 = 0.2$ using (4.24).

In terms of the approximating lognormal RVs, the expression for the SINR of a single user from (4.2) can be written as

$$SINR_j^{mrc} \triangleq \frac{P_t Y}{P_t R + 1}, \tag{4.26}$$

where $Y \sim \text{Log-}\mathcal{N}(\mu_X, \sigma_X^2)$ is obtained by either the moment matching method or the MGF-based method and $R \sim \text{Log-}\mathcal{N}(\mu_b, \sigma_b^2)$ is obtained as stated above. Multiplication of a lognormal RV by P_t adds $\xi \log_e P_t$ to the mean value of the associated Gaussian RV whereas the addition of 1 to the RV R in the denominator of (4.26) simply adds unity to the expected value of RV R.

The SINR of the jth user in (4.26) can now be expressed as a ratio of two independent lognormal RVs,

$$SINR_j^{mrc} \triangleq \frac{Log\mathcal{N}(\mu_X + \xi \log_e P_t, \sigma_X^2)}{Log\mathcal{N}(\mu_b + \xi \log_e P_t, \sigma_b^2)} \tag{4.27}$$

The ratio of two lognormals is again a lognormal RV. Therefore

$$SINR_j^{mrc} \sim Log\mathcal{N}(\mu_X - \mu_b, \sigma_X^2 + \sigma_b^2) \tag{4.28}$$

4.3 Simulation results for lognormal approximation of SINR

In this section, we plot the CDF and the CCDF of SINR to verify the accuracy of the proposed lognormal approximation of SINR.

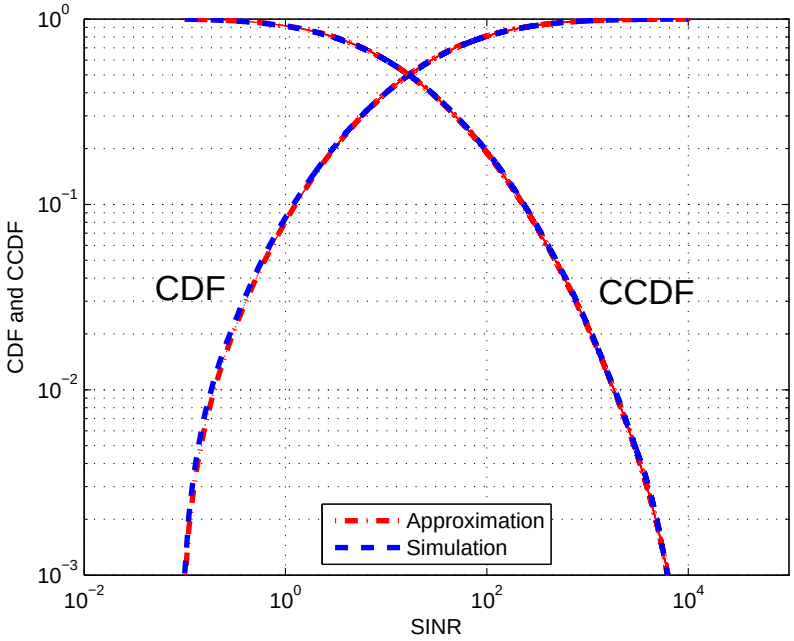

Figure 4.3: CDF and CCDF of SINR

Fig. 4.3 plots the CDF and the CCDF of SINR for an MRC receiver. The SNR in the numerator of (4.26) is obtained through the moment matching approach. We choose 500 BS antennas, $P_t = 10$, $\mu_{(dB)} = 0$, $\sigma_{(dB)} = 8$ and 10 users to plot the results. We also assume that all the users suffer from identical shadowing. Fig. 4.3 shows a good match between the simulation results and approximation results. Like the SNR approximation, there is a greater accuracy in approximating the CCDF of SINR as compared to the CDF of SINR. This implies that the proposed lognormal approximation of SINR can be used as an accurate tool to calculate the outage probability of the system.

Chapter 5

Analysis of ZF and MMSE Receivers

In this chapter we analyze the zero forcing (ZF) and minimum mean squared error (MMSE) receivers for a massive MIMO system operating a composite Rayleigh fading-lognormal shadowing environment. Based on the analysis of MRC receiver, we approximate the SINRs of ZF and MMSE receivers by lognormal RVs.

5.1 ZF Receiver

The detector matrix $\boldsymbol{A}$ for a ZF receiver is given by

$$\boldsymbol{A} = \boldsymbol{G}\left(\boldsymbol{G}^H\boldsymbol{G}\right)^{-1}. \tag{5.1}$$

Therefore, $\boldsymbol{A}^H\boldsymbol{G} = \boldsymbol{I}_K$ and $\boldsymbol{a}_j^H\boldsymbol{g}_k = \delta_{jk}$ where $\delta_{jk} = 1$ for $j = k$ and 0 otherwise.

From (3.7), the SINR of jth user in case of ZF receiver can then be written

as

$$\begin{aligned} SINR_j^{zf} &= \frac{P_t|\boldsymbol{a}_j^H\boldsymbol{g}_j|^2}{P_t\sum_{k=1,k\neq j}^{K}|\boldsymbol{a}_j^H\boldsymbol{g}_k|^2+\|\boldsymbol{a}_j\|^2} \\ &\triangleq \frac{P_t}{\|\boldsymbol{a}_j\|^2} \end{aligned} \tag{5.2}$$

Since $\|\boldsymbol{a}_j\|^2 = \boldsymbol{a}_j^H\boldsymbol{a}_j$ and $\boldsymbol{A} = \boldsymbol{G}\left(\boldsymbol{G}^H\boldsymbol{G}\right)^{-1}$ for a ZF receiver, therefore

$$\boldsymbol{A}^H\boldsymbol{A} = \left(\boldsymbol{G}^H\boldsymbol{G}\right)^{-1}\left(\boldsymbol{G}^H\boldsymbol{G}\right)\left(\boldsymbol{G}^H\boldsymbol{G}\right)^{-1} \triangleq \left(\boldsymbol{G}^H\boldsymbol{G}\right)^{-1} \tag{5.3}$$

and

$$\|\boldsymbol{a}_j\|^2 = \boldsymbol{a}_j^H\boldsymbol{a}_j = \left[\left(\boldsymbol{G}^H\boldsymbol{G}\right)^{-1}\right]_{jj}. \tag{5.4}$$

From (5.2) and (5.4), the SINR is then given as

$$SINR_j^{zf} = \frac{P_t}{\left[\left(\boldsymbol{G}^H\boldsymbol{G}\right)^{-1}\right]_{jj}}. \tag{5.5}$$

If we denote $\boldsymbol{G}_j$ to be the submatrix obtained after omitting the jth column from $\boldsymbol{G}$, then,

$$\begin{aligned} \left[\left(\boldsymbol{G}^H\boldsymbol{G}\right)^{-1}\right]_{jj} &= \frac{1}{\boldsymbol{g}_j^H\boldsymbol{g}_j - \boldsymbol{g}_j^H\boldsymbol{G}_j\left(\boldsymbol{G}_j^H\boldsymbol{G}_j\right)^{-1}\boldsymbol{G}_j^H\boldsymbol{g}_j} \\ &\triangleq \frac{1}{\nu_j\left(\boldsymbol{h}_j^H\boldsymbol{h}_j - \boldsymbol{h}_j^H\boldsymbol{H}_j\left(\boldsymbol{H}_j^H\boldsymbol{H}_j\right)^{-1}\boldsymbol{H}_j^H\boldsymbol{h}_j\right)}. \end{aligned} \tag{5.6}$$

Substituting (5.6) in (5.5), we obtain the SINR of ZF receiver as

$$\begin{aligned} SINR_j^{zf} &= P_t\nu_j\left(\boldsymbol{h}_j^H\boldsymbol{h}_j - \boldsymbol{h}_j^H\boldsymbol{H}_j\left(\boldsymbol{H}_j^H\boldsymbol{H}_j\right)^{-1}\boldsymbol{H}_j^H\boldsymbol{h}_j\right) \\ &\triangleq P_t\nu_j S_j. \end{aligned} \tag{5.7}$$

where $S_j = \left(\boldsymbol{h}_j^H\boldsymbol{h}_j - \boldsymbol{h}_j^H\boldsymbol{H}_j\left(\boldsymbol{H}_j^H\boldsymbol{H}_j\right)^{-1}\boldsymbol{H}_j^H\boldsymbol{h}_j\right)$.

In case of Rayleigh fading, S_j follows a gamma distribution [35], i.e., $S_j \sim \Gamma(M-K+1,1)$. From (5.7), the SINR for a ZF receiver also follows a gamma-lognormal product distribution like the SNR of MRC receiver. Using the

approach devised in section 4.1 for the SNR of MRC receiver, we approximate the SINR of ZF receiver by a lognormal RV such that

$$SINR_j^{zf} \sim Log\mathcal{N}(\mu_{zf}, \sigma_{zf}^2)$$

where

$$\mu_{zf} = \xi\psi(M-K+1) + \mu_{dB} + \xi \log_e P_t$$

$$\sigma_{zf}^2 = \sigma_{dB}^2 + \xi^2\zeta(2,(M-K+1)). \tag{5.8}$$

and

$$\psi(M-K+1) = -0.5772 + \sum_{k=1}^{M-K} \frac{1}{k}$$

$$\zeta(2,(M-K+1)) = \sum_{k=0}^{\infty} \frac{1}{(M-K+1+k)^2} \tag{5.9}$$

The SINR of the jth user, in case of ZF receiver, is affected by the small-scale fading coefficients of all the users and the large-scale fading coefficient of only the jth user. The ZF receiver suppresses the shadowing of all the interfering users.

5.2 MMSE Receiver

The detector matrix $\boldsymbol{A}$ for an MMSE receiver is given by $\boldsymbol{A} = \boldsymbol{G}\left(\boldsymbol{G}^H\boldsymbol{G} + \frac{1}{P_t}\boldsymbol{I}_K\right)^{-1}$. From [39], the jth column of $\boldsymbol{A}$ is given as

$$\boldsymbol{a}_j = \frac{\boldsymbol{F}\boldsymbol{g}_j}{1 + \boldsymbol{g}_j^H\boldsymbol{F}\boldsymbol{g}_j} \tag{5.10}$$

where $\boldsymbol{F} = \left(\boldsymbol{G}_j\boldsymbol{G}_j^H + \frac{1}{P_t}\boldsymbol{I}_M\right)$ and $\boldsymbol{G}_j$ is the submatrix obtained after omiting the jth column of $\boldsymbol{G}$. Substituting (5.10) into (3.7), we get the SINR of jth user as

$$SINR_j^{mmse} = \frac{1}{\left[\left(P_t\, \boldsymbol{G}^H \boldsymbol{G} + \boldsymbol{I}_K\right)^{-1}\right]_{jj}} - 1. \tag{5.11}$$

The PDF of $SINR_j^{mmse}$ does not exist in a closed-form. However, when the channel impairments include Rayleigh fading only, the distribution of $SINR_j^{mmse}$ can be approximated by a Gaussian distribution [40], [41] or a gamma distribution [42]-[44]with a only a certain degree of accuracy.

The SINR in case of MMSE receiver can be decomposed into two independent RVs [36], such that

$$SINR_j^{mmse} = SINR_j^{zf} + T_j. \tag{5.12}$$

In the presence of Rayleigh fading only, it is shown in [36] that $T_j \sim \Gamma(\tilde{c}, \tilde{d})$, where $\tilde{c} = \frac{(K-1)\alpha^2}{\beta^2}$, $\tilde{d} = \frac{\beta^2}{\alpha}$ and α and β are determined by solving the following equations:

$$\alpha = \frac{1}{MP_t\left(1 - \frac{K-1}{M} + \frac{K-1}{M}\alpha\right) + 1}$$

$$\beta\left(1 + \frac{(K-1)\,P_t}{\left(MP_t\left(1 - \frac{K-1}{M} + \frac{K-1}{M}\alpha\right) + 1\right)^2}\right) = \frac{(K-1)\left(P_t\alpha + \frac{1}{(K-1)}\right)}{\left(MP_t\left(1 - \frac{K-1}{M} + \frac{K-1}{M}\alpha\right) + 1\right)^2} \tag{5.13}$$

When all the users experience same shadowing, ν, under a composite fading environment, T_j follows a gamma-lognormal product distribution. Following a similar course of action like the SNR of MRC receiver, we approximate T_j by a lognormal RV such that $T_j \sim Log\mathcal{N}(\mu_T, \sigma_T^2)$

where

$$\mu_T = \xi\left\{\psi(\tilde{c}) + \log_e(\tilde{d})\right\} - \mu_{dB} + \xi\log_e(P_t), \tag{5.14}$$

and

$$\sigma_T^2 = \xi^2\zeta(2, \tilde{c}) + \sigma_{dB}^2. \tag{5.15}$$

From (5.12), $SINR_j^{mmse}$ is the addition of two lognormal RVs. The sum of lognormal RVs is again approximated by another lognormal RV by the MGF- based method as in section 4.2.

Chapter 6

Simulation Results and Performance Analysis

In this chapter, we plot the results for a massive MIMO system under a composite fading environment. We then analyze these results from different perspectives to establish meaningful and valuable insights. We first verify the accuracy of the proposed lognormal approximations of SINR for all the three receivers.

Fig. 6.1 shows that the SINR for all the three receivers can be very well approximated by a lognormal distribution. There is very close match between the simulated and the analytically obtained CCDF of SINRs. Here, we have chosen unit P_t and 10 users. For simulations, we multiplied the Rayleigh and lognormal RVs according to (3.7) and averaged them over 10^7 Monte-Carlo trials. Since, we have assumed 500 BS antennas, the CCDF of the SINR for ZF and MMSE receivers appears to be identical.

Before proceeding for further results, we define here two notations, the *outage probability* and the *SNR margin*. When the SINR follows a lognormal

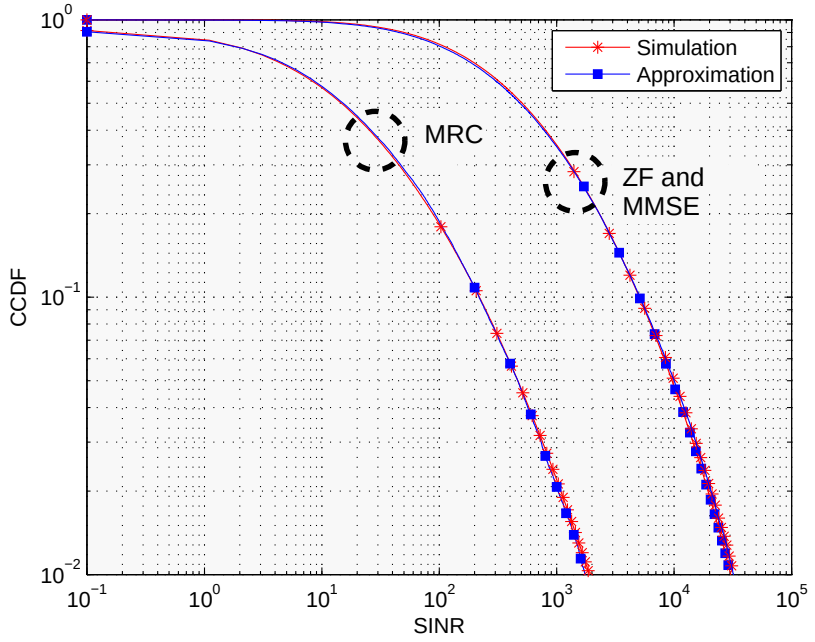

Figure 6.1: CCDF of SINR for MRC, ZF and MMSE receivers with 10 users and 500 BS antennas. All users experience identical shadowing ($\mu_{dB} = 0$, $\sigma_{dB} = 8$ and $P_t = 0$ dBm).

distribution, the outage probability, $\mathcal{O}$, is given by

$$\mathcal{O} = \mathbb{P}\left\{SINR \leq \tau\right\} = Q\left(\frac{\mu_Y - 10\log_{10}\tau}{\sigma_Y}\right), \tag{6.1}$$

where Q-function gives the tail probability; $Q(x) = \frac{1}{\sqrt{2\pi}}\int_x^\infty \exp\left(\frac{-y^2}{2}\right)dy$, μ_Y and σ_Y are the mean and standard deviation, in dB, associated with the approximating RV Y, respectively, and τ is the modulation dependent threshold. The SNR margin, ρ, is interpreted as the normalized transmit SNR of a user and is given by $\rho = \frac{P_t}{\tau}$.

Fig. 6.2 compares the performance of the three receivers in terms of the outage probability. The ZF and MMSE receivers out perform the MRC receiver under identical conditions because the MRC receiver does not cater

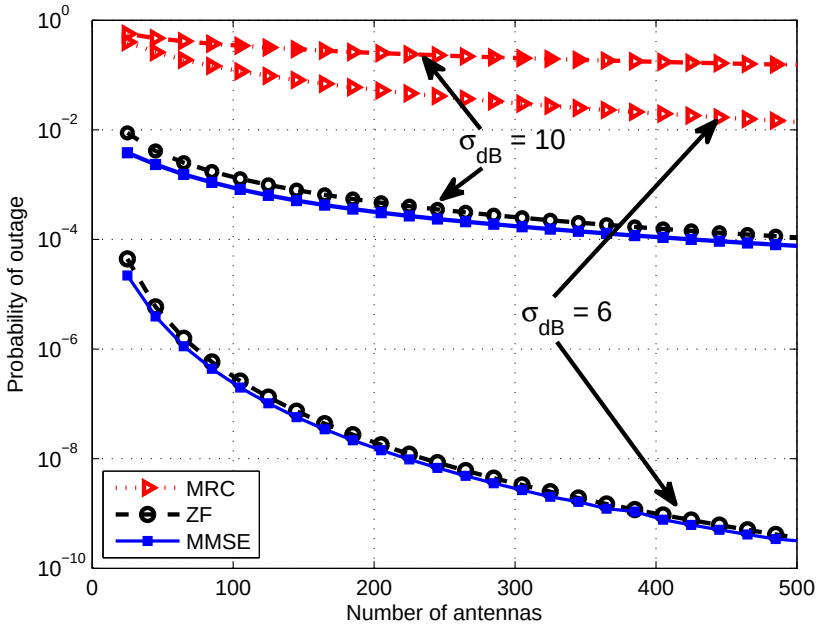

Figure 6.2: Outage probability for MRC, ZF and MMSE receivers with 10 users. All users experience identical shadowing ($\mu_{dB} = 0$ and $\rho = 10dB$).

for interference and noise. It simply adds up the received signals from all the users. The outage of ZF receiver is lower bounded by the MMSE receiver. In the limit when $\rho \to \infty$, the performance of ZF receiver tends to that of the MMSE receiver. The difference between the outages of MRC and MMSE receivers alleviates as the σ_{dB} of shadowing increases. For example, at 100 BS antennas and 6 dB shadowing, there is a difference of 99.75% between the outages of MMSE and MRC receivers as compared to an approximate 100% difference at 10 dB shadowing. Moreover, there is a reduction of only 64.3% in the outage of MRC receiver when σ_{dB} varies from 10 dB to 6 dB at 100 antennas as compared to a reduction of almost 99.97% in the outage of an MMSE receiver. This shows that shadowing is an important channel param-

eter that should be catered for carefully and the choice of receiver should be made according to the shadowing conditions and appropriate shadow margin should be provided.

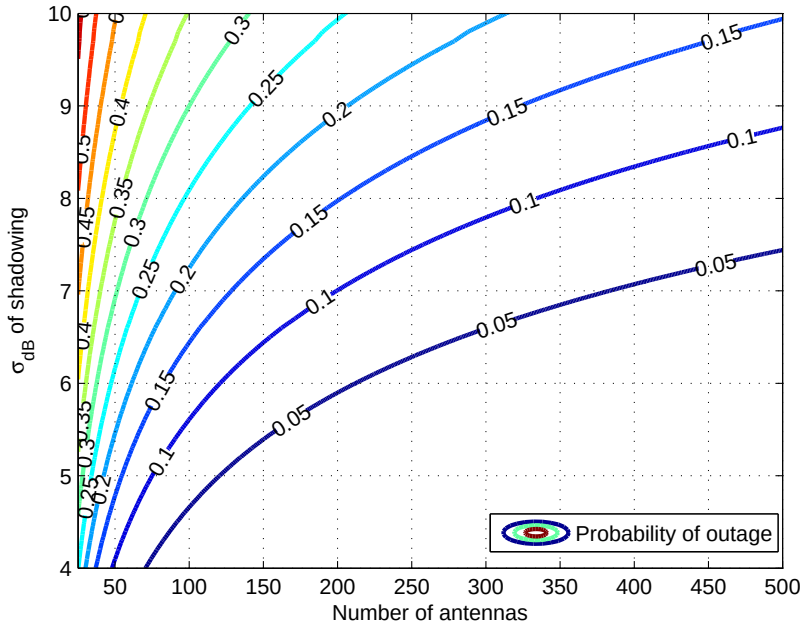

Figure 6.3: Probability of outage for an MRC receiver as a function of number of antennas and σ of shadowing. All users experience identical shadowing ($\mu_{dB} = 0$, $K = 10$ and $\rho = 10dB$).

Fig. 6.3 plots the outage probability of the MRC receiver for 10 users as a function of the number of antennas and σ_{dB}. The results quantify the number of antennas required to achieve a specific quality of service (QoS) at a fixed SNR margin and a certain σ. The QoS is the outage probability in our case. To achieve a QoS of 0.02 under 8 dB shadowing at $\rho = 10$ dB, 135 antennas are required at the BS, whereas 334 antennas are needed to achieve a QoS of 0.1.

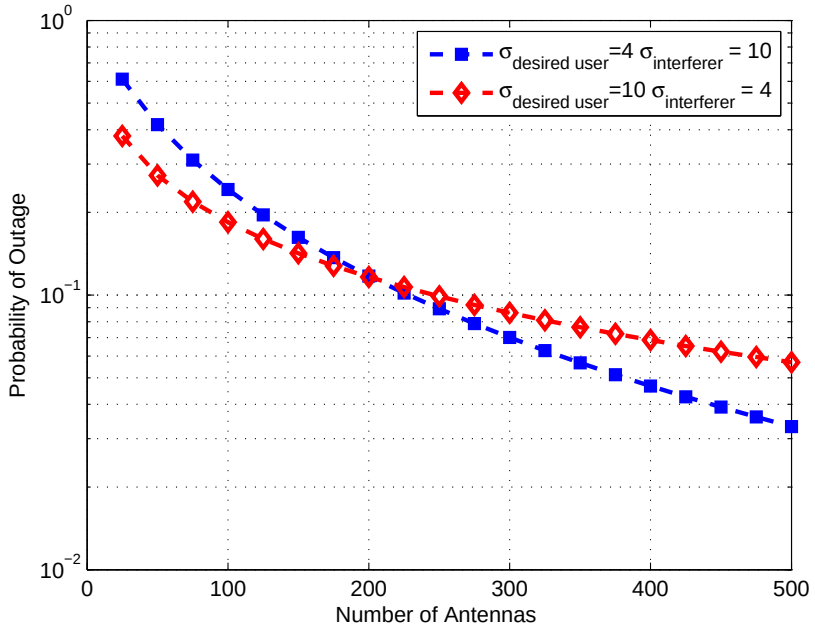

Figure 6.4: Probability of outage for an MRC receiver in two different scenarios with 10 users ($\mu_{dB} = 0$, $\rho = 10$ dB).

Fig. 6.4 plots the outage probability of the MRC receiver for two different scenarios with 10 users each. In the first scenario, the desired user suffers light shadowing and the interferers are severely shadowed, whereas it is vice versa in the other scenario. It can be seen that when the desired user is severely shadowed, the user experiences less outage for lesser number of antennas. This is because the shadowing phenomenon models the fluctuations in the received power around a certain mean; the average SINR defines the mean which is a function of number of antennas. These fluctuations become large when σ of shadowing is increased. Therefore, on the average, the received power crosses a set threshold more often and the user experiences less outage. Under such channel conditions, one can get a favourable shadowing outcome

at lesser number of antennas, which eventually reduces the outage probability. This is contrary to the case where the channel consists only of small-scale fading and only an increase in the number of BS antennas averages out the fading effect and reduces the outage probability. In Fig. 6.4, both the scenarios have the same outage probability at 200 BS antennas. This gives an estimate of the shadow margin that needs to be kept at the user side. For different channel conditions, the shadow margin will be different.

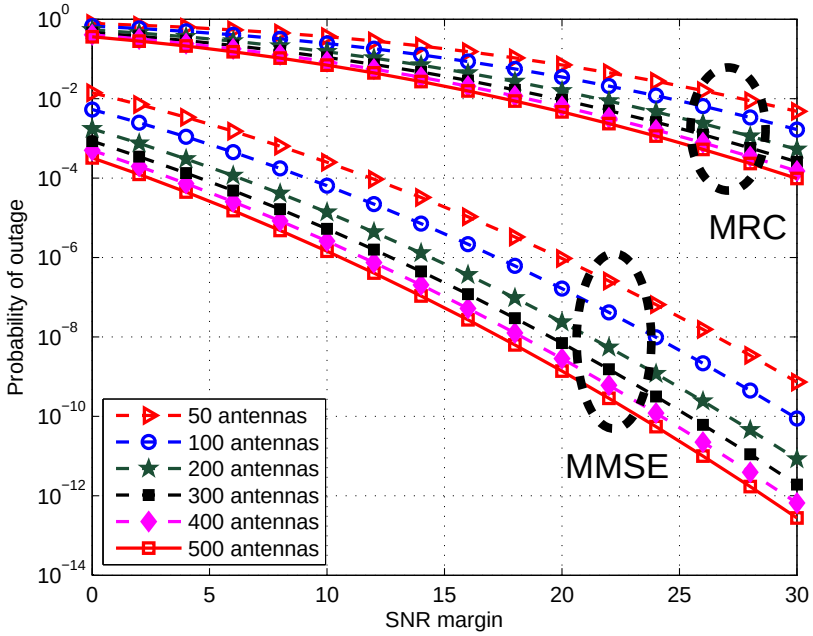

Figure 6.5: Effect of SNR margin on the probability of outage for MRC and MMSE receivers with 10 users each. All users experience identical shadowing ($\mu_{dB} = 0, \sigma_{dB} = 8$)

Fig. 6.5 shows that the reduction in the outage is more pronounced for an MMSE receiver as compared to an MRC receiver when M is increased at a constant ρ. For example, at ρ =15 dB, there is a 78.89% decrease in the

outage of MMSE receiver when M is increased from 50 to 100 as compared to a 41.89% decrease for an MRC receiver. The diminishing trend of reduction in the outage can also be observed as M is increased. The reduction in outage for a specific ρ is more prominent when we increase M from 50 to 100 as compared to the case when we increase M from 400 to 500. This is because the diversity gain of the system does not increase linearly with the increase in number of antennas. Moreover, there is a trade-off between the SNR margin and the number of antennas. If either of the quantities is reduced, then the other quantity needs to be increased in order to maintain a specific QoS.

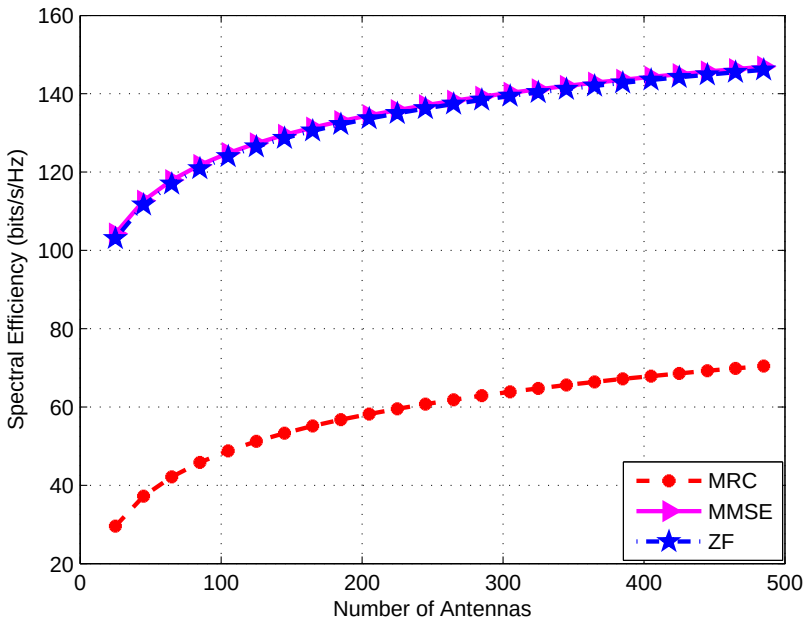

Figure 6.6: Spectral efficiency of MRC, ZF and MMSE receivers with 10 users ($\mu_{dB} = 0$, $\sigma_{dB} = 8$ and $\rho = 10dB$).

Fig. 6.6 illustrates the spectral efficiency of the three receivers as the

number of antennas is increased. The rate of a single user is given by

$$\mathcal{R}_j \;=\; \mathbb{E}\left\{\log_2(1+SINR_j)\right\}. \tag{6.2}$$

By using Jensen's inequality, we obatin the lower bound on rate as

$$\mathcal{R}_j \geq \log_2(1+\mathbb{E}\left\{SINR_j\right\}). \tag{6.3}$$

Since $SINR_j \sim Log\mathcal{N}(\mu,\sigma^2)$, where μ and σ^2 for the MRC, ZF and MMSE receivers are obtained from chapters 4 and 5, therefore,

$$\mathbb{E}\left\{SINR_j\right\} = 10^{(0.1\mu)}\exp\frac{\sigma^2}{2}\left(\frac{\log_e 10}{10}\right)^2. \tag{6.4}$$

The spectral efficiency of the system is then given by

$$\eta = \sum_{j=1}^{K}\mathcal{R}_j. \tag{6.5}$$

The ZF and MMSE receivers are more spectrally efficient than the MRC receiver.

Chapter 7

Conclusion and Future Work

This chapter summarizes the contributions of this research and also suggests some possible future directions.

In this thesis, we developed a system model for a massive MIMO system operating under a composite Rayleigh fading-lognormal shadowing environment with perfect CSI and assuming identical shadowing at all of the BS antennas for a particular user . We then analyzed three linear receivers, namely MRC, ZF and MMSE under such operating conditions. We established that the SNR of an MRC receiver follows a gamma-lognormal product distribution under these channel conditions. Since the PDF of gamma-lognormal product distribution does not exist in a closed-form, we proposed two approximation methods to approximate the SNR of an MRC receiver by a lognormal RV.

The PDF of SINR of these three receivers does not exist in a closed-form. Based on the lognormal approximation of SNR, we approximated the SINR of MRC, ZF and MMSE receivers by lognormal RVs and showed that there is a close match between the simulated SINRs and the lognormal approximations of SINRs of the three receivers.

Approximation of SINR by a lognormal RV helps in establishing closed-form expressions for the outage probability and the rate of a user. We also provided closed-form expressions for the outage probability and system capacity of a massive MIMO system under a composite fading environment. We compared the performance of the three receivers in terms of outage probability and the capacity of the system and showed that the MMSE receiver outperforms the MRC receiver and the performance of ZF receiver is almost the same as the performance of the MMSE receiver. We also quantified the effects of shadowing on these systems and showed that the large-scale fading, unlike small-scale fading, does not average out by increasing the number of antennas. Lower bounds on uplink achievable rates have also been established.

As possible future directions of this research work, we suggest the following:

- Extending the devised approach to a multi-cell scenario.
- Incorporating the effects of pilot contamination.
- Working with imperfect CSI rather than perfect CSI.
- Assuming correlated shadowing at only a subset of BS antennas rather than all of the BS antennas.

Bibliography

[1] D. Gesbert , M. Shafi , D. Shiu, P. Smith and A. Naguib, "From theory to practice: An overview of space-time coded MIMO wireless systems", *IEEE J. Sel. Areas Commun.* vol. 21, no. 3, pp. 281-302. 2003.

[2] A. J. Paulraj, D. A. Gore, R. U. Nabar and H. Bolcskei, "An overview of MIMO communications - A key to gigabit wireless", *Proc. of the IEEE*, vol. 92, pp. 198-218. 2004.

[3] E. G. Larsson, "MIMO detection methods: How they work," *IEEE Signal Process. Mag.*, vol. 26, no. 3, pp. 9195, May 2009.

[4] J. Jaldén and B. Ottersten, "On the complexity of sphere decoding in digital communications," *IEEE Trans. Signal Process.*, vol. 53, no. 4, pp. 14741484, Apr. 2005.

[5] T. L. Marzetta, "Noncooperative cellular wireless with unlimited numbers of base station antennas," *IEEE Trans. Wireless. Commun.,* vol. 9, no. 11, pp. 3590-3600, Nov. 2010.

[6] F. Rusek, D. Persson, B. K. Lau, E. G. Larsson, T. L. Marzetta, O. Edfors, and F. Tufvesson,"Scaling up MIMO: Opportunities and challenges

with very large arrays," *IEEE Signal Process. Mag.,* vol. 30, pp. 40-60, Jan. 2013.

[7] H. Yang and T. L. Marzetta, "Performance of conjugate and zero-forcing beamforming in large-scale antenna systems," *IEEE J. Sel. Areas Commun.,* vol. 31, no. 2, pp. 172-179, Feb. 2013.

[8] E. Larsson, F. Tufvesson, O. Edfors, T. Marzetta, "Massive MIMO for next generation wireless systems," *IEEE Commun. Mag.*, vol. 52, no. 2, pp.186-195, Feb. 2014.

[9] H. Q. Ngo, E. G. Larsson, T. L. Marzetta, "Energy and spectral efficiency of very large multiuser MIMO systems," *IEEE Trans. Wireless Commun.*, vol. 61, no. 4, pp. 1436-1449, April 2013.

[10] C. Studer, E. G. Larsson, "PAR-aware large-scale multi-user MIMO-OFDM downlink," *IEEE J. Sel. Areas Commun.*, vol. 31, no. 2, pp. 303-313, Feb. 2013.

[11] J. Hoydis, S. ten Brink, and M. Debbah, Massive MIMO in the UL/DL of cellular networks: How many antennas do we need? *IEEE J. Sel. Areas Commun.*, vol. 31, no. 2, pp. 160171, Feb. 2013.

[12] N. Krishnan, R. Yates, N. Mandayam, "Uplink linear receivers for multi-cell multi-user MIMO with pilot contamination: Large system analysis," *IEEE Trans. Wireless Commun.,* doi: 10.1109/TWC.2014.2320914.

[13] J. Jose, A. Ashikhmin, T. L. Marzetta, S. Vishwanath, "Pilot contamination and precoding in multi-cell TDD systems," *IEEE Trans. Wireless Commun.*, vol. 10, no. 8, pp. 2640-2651, Aug. 2011.

[14] N. B. Mehta, J. Wu, A. F. Molisch, and J. Zhang, "Approximating a sum of random variables with a lognormal," *IEEE Trans. Wireless Commun.,* vol. 6, pp. 2690-2699, July 2007.

[15] M. A. Kamath and B. L. Hughes, "The asymptotic capacity of multiple antenna Rayleigh-fading channels," *IEEE Trans. Inf. Theory,* vol. 51, no. 12, pp. 43254333, Dec. 2005.

[16] H. Shin, M. Z. Win, and M. Chiani, "Asymptotic statistics of mutual information for doubly correlated MIMO channels," *IEEE Trans. Wireless Commun.,* vol. 7, no. 2, pp. 562573, Feb. 2008.

[17] A. Grant, "Rayleigh fading multi-antenna channels," *EURASIP J. Appl. Signal Process.,* vol. 3, pp. 316329, 2002.

[18] X. Mestre, J. R. Fonllosa, and A. P. Zamora, "Capacity of MIMO channels: Asymptotic evaluation under correlated fading," *IEEE J. Sel. Areas Commun.,* vol. 21, pp. 829838, Jun. 2003.

[19] C. Chuah, D. N. C. Tse, J. M. Kahn, and R. A. Valenzuela, "Capacity scaling in MIMO wireless systems under correlated fading," *IEEE Trans. Inf. Theory,* vol. 48, no. 3, pp. 637650, Mar. 2002.

[20] S. K. Jayaweera and H. V. Poor, "On the capacity of multiple-antenna systems in Rician fading," *IEEE Trans. Wireless Commun.,* vol. 4, no. 3, pp. 11021111, May 2005.

[21] X. W. Cui, Q. T. Zhang, and Z. M. Feng, "Generic procedure for tightly bounding the capacity of MIMO correlated Rician fading channels," *IEEE Trans. Commun.,* vol. 53, pp. 890898, May 2005.

[22] M. R. Mckay and I. B. Collings, "General capacity bounds for spatially correlated Rician MIMO channels," *IEEE Trans. Inf. Theory,* vol. 51, no. 9, pp. 31213145, Sep. 2005.

[23] S. Jin, X. Gao, and X. You, "On the ergodic capacity of rank-1 Rician fading MIMO channels," *IEEE Trans. Inf. Theory,* vol. 53, no. 2, pp. 502517, Feb. 2007.

[24] M. Kang and M. S. Alouini, "Capacity of MIMO Rician channels," *IEEE Trans. Wireless Commun.,* vol. 5, no. 1, pp. 112122, Jan. 2006.

[25] C. Zhong, K.-K. Wong, and S. Jin, "Capacity bounds for MIMO Nakagami-m fading channels," *IEEE Trans. Signal Process.,* vol. 57, no. 9, pp. 3613-3623, Sep. 2009.

[26] A. Yang, Z. He, C. Xing, Z. Fei, and J. Kuang, "The role of large-scale fading in uplink massive MIMO systems." arXiv preprint arXiv:1406.3164, 2014.

[27] A. Laourine, M. -S. Alouini, S. Affes, and A. Stéphenne, "On the capacity of generalized-$\mathcal{K}$ fading channels," *IEEE Trans. Wireless Commun.,* vol. 7, no. 7, pp. 2441-2445, Jul. 2008.

[28] K. Li, X. Song, M. O. Ahmad, and M. N. S. Swamy, "An improved multicell MMSE channel estimation in a massive MIMO system," *Int. J. Antennas Propag.*, 2014, doi:10.1155/2014/387436.

[29] M. Bacha, S. A. Hassan, "Performance analysis of linear cooperative multi-hop networks subject to composite shadowing fading," *IEEE Trans. Wireless Commun.*, vol. 12, no. 11, pp. 5850-5858, Nov. 2013.

[30] A. F. Molisch, *Wireless Communication*. Wiley-IEEE Press, 2005.

[31] G. L. Stuber, *Principles of Mobile Communications*. Kluwer Academics Publishers, 1996.

[32] Simon R. Saunders, *Antennas and Propagation for Wireless Communication Systems*, John Wiley and Sons, LTD, 1999.

[33] B. Wang, Y. Chang, D. Yang, "On the SINR in massive MIMO networks with MMSE receivers," *IEEE Commun. Letters*, vol.18, no.11, pp. 1979-1982, Nov. 2014.

[34] H. Q. Ngo, M. Matthaiou, T. Q. Duong, E. G. Larsson, "Uplink performance analysis of multicell MU-SIMO systems with ZF receivers," *IEEE Trans. Veh. Technol.*, vol. 62, no. 9, pp. 4471-4483, Nov. 2013.

[35] Y. Jiang, M. Varanasi, and J. Li, "Performance analysis of ZF and MMSE equalizers for MIMO systems: An in-depth study of the high SNR regime," *IEEE Trans. Inf. Theory*, vol. 57, no. 4, pp. 2008-2026, Apr. 2011.

[36] P. Li , D. Paul , R. Narasimhan and J. Cioffi, "On the distribution of SINR for the MMSE MIMO receiver and performance analysis," *IEEE Trans. Inf. Theory*, vol. 52, no. 1, pp. 271-286, 2006.

[37] T. S. Rappaport, *Wireless Communications: Principles and Practice*. Prentice-Hall, 1996.

[38] B. Sklar, "Rayleigh fading channels in mobile digital communications systems part I: Characterization," *IEEE Commun. Mag.*, vol. 35, no. 7, pp. 90100, Jul. 1997.

[39] N. Kim, Y. Lee and H. Park, "Performance analysis of MIMO system with linear MMSE receiver", *IEEE Trans. Wireless Commun.*, vol. 7, no. 11, pp. 4474-4478, 2008.

[40] Y. -C. Liang, G. Pan and Z. D. Bai, "Asymptotic performance of MMSE receivers for large systems using random matrix theory", *IEEE Trans. Inf. Theory*, vol. 53, no. 11, pp. 4173-4190, Nov. 2007.

[41] A. Kammoun et al. "A central limit theorem for the SINR at the LMMSE estimator output for large dimensional systems", *IEEE Trans. Inf. Theory*, vol. 55, no. 11, pp. 5048-5063, Nov. 2009.

[42] H. Li and A. G. Armada, "Bit error rate performance of MIMO MMSE receivers in correlated Rayleigh flat-fading channels," *IEEE Trans. Veh. Technol.*, vol. 60, no. 1, pp. 313-317, Jan. 2011.

[43] A. G. Armada, L. Hong and A. Lozana, "Bit loading for MIMO with statistical channel information at the transmitter and ZF receivers," *Proc. IEEE Int. Conf. Commun.*, pp. 3836-3840, 2009.

[44] A. Kammoun, M. Kharouf, W. Hachem and J. Najim, "BER and outage probability approximations for LMMSE detectors on correlated MIMO channels," *IEEE Trans. Inf. Theory*, vol. 55, no. 10, pp. 4386-4397, 2009.